Molecular Catalysis 510 (2021) 111667

Contents lists available at ScienceDirect

Molecular Catalysis

journal homepage: www.journals.elsevier.com/molecular-catalysis

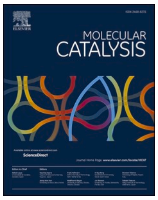

Comparative account of catalytic activity of Ru- and Ni-based nanocomposites towards reductive amination of biomass derived molecules

Tejas A. Gokhale, Amol B. Raut, Bhalchandra M. Bhanage *

Department of Chemistry, Institute of Chemical Technology, Nathalal Parekh Marg, Matunga, Mumbai, 400019 India

ARTICLE INFO

Keywords:
Biomass
Furfural
Ammonia
Reductive amination
Montmorillonite

ABSTRACT

This work includes an effective comparison of metallic ruthenium and nickel nanoparticles loaded on montmorillonite clay (MMT) for reductive amination reaction of biomass-derived molecules. It comprises an eco-friendly reaction using water as a solvent, utilizing molecular hydrogen and liquor ammonia (25% aq. solution) for the synthesis of primary amines from bio-derived aldehydes within 3–10 h of reaction time. Various parameters such as temperature, hydrogen pressure, substrate/ammonia concentration ratio, and reaction time were optimized while comparing the selectivity of primary amines for both catalysts. The applicability scope of these catalysts was explored with a library of aryl and heterocyclic aldehydes. The reductive amination of crude furfural extracted from biomass feedstock (rice husk) and pure xylose sugar was tested, showing yields in the range of 11–36%, to show the wider industrial scope of both nanocomposites. Gram scale conversion was also carried out to showcase the bulk scalability of the Ru/MMT catalyst.

Introduction

Biomass extracted chemicals and their further processed and derivatized compounds are mounting in their importance over the last two decades. With a major emphasis on finding alternatives over limited and environment polluting fossil fuel feedstocks, lignocellulosic biomass has emerged as the prominent and renewable feedstock source for platform chemicals for further conversion to bio-fuels [1,2] and value-added chemical syntheses [3,4]. Amongst these molecules, furfural [5] and 5-hydroxymethyl furfural (HMF) [6] have been the most explored due to their facile but variable conversions into chemicals with a wide array of applications [7,8].

Amines are a vital class of compounds having varied applications in the field of agrochemical agents, polymer substrates, pharmaceutical ingredient syntheses [9]. Reductive amination is an economic reaction process for the synthesis of primary [10], secondary [11–15], and ternary functionalized amines [16–18] using molecular hydrogen or other hydrogen sources with the former having advantages such as high atom economy, absence of toxic by-products, and industrial scalability [19,20]. Moreover, ammonia is used for primary amine synthesis, factoring in it being a bulk manufactured, low-cost commodity chemical. The challenging obstacle involving the primary amine synthesis is abstaining from the pathway towards the conversion of primary amines to secondary amines [21]. Moreover, a limited number of reports have been published showing this reaction in biomass extracted molecules such as furfural and other derivatives.

The recent reports have presented heterogeneous catalysts that show appreciable catalytic activity towards the conversion of aldehyde groups to primary as well as secondary amines. Maya et al. studied reductive amination of furfural derivatives using variable metal (Rh, Pd, Pt) containing commercially available catalysts with differing selectivity towards primary and secondary amines with now widely accepted reaction pathway [22]. Liang et al. reported zirconia supported catalytic system to synthesize a library of aminated compounds [23]. Hara and his co-workers evaluated the synergistic electronic effects of Ru nanoparticles with Nb_2O_5 support and its resultant interpretation in terms of reductive amination of furanic aldehydes [24]. Furthermore, his team optimized the same catalyst by employing niobic acid (Nb_2O_5. x H_2O) in place of Nb_2O_5 in the context of increasing Lewis acidic sites on the support surface [25]. His work also includes the use of templated ruthenium nanoparticles for the reductive amination process [26]. Feng Shi and his co-workers applied a relatively high loading of nickel on alumina with optimal reaction conditions for the process [27]. Ortiz et al. optimized the work towards the formation of secondary amines by one-pot two-step synthesis from its nitro substrates as the starting point using Pd/C and Pd/Al_2O_3 catalyst synthesized by wet impregnation

---

* Corresponding author.
E-mail address: bm.bhanage@ictmumbai.edu.in (B.M. Bhanage).

https://doi.org/10.1016/j.mcat.2021.111667
Received 8 December 2020; Received in revised form 18 May 2021; Accepted 19 May 2021

method [11]. Zhang and his group showed conversion of nitriles to primary amines by using nickel supported on doped carbon structure [28]. His group further loaded cobalt on nitrogen-doped carbon to achieve good yields using carbonyl compounds for reductive amination reaction [29]. Jv et al. showed decent conversions with pH-controlled, ligand stabilized Pd nanoparticles for the reductive amination of aryl aldehydes [30]. Recently, Xie et al. used ruthenium loaded on titanium phosphate exhibited good yields in the case of furfural substrate in 24 h of reaction time. [31]

Mainly, the focus in this sub-branch of the field has been about optimizing and testing the support material used for loading of the nanoparticles as it holds significant standing in regards to the performance of the catalyst. One of the environmentally benign, inexpensive, and omnipresent support materials, i.e., Montmorillonite clay (MMT) might be a good choice as 1) It has a lamellar based structure in its magnesium aluminum silicate assembly, translating into higher than usual surface area when exfoliated 2) High tolerance temperature and pressure stability 3) Present electrostatic force due to the negatively charged surface, which holds the nanoclusters in place reducing any metal leaching and 4) Mixture of weak to moderate surface Brønsted and Lewis acidic sites [32,33].

Present work aids in establishing a nexus between the inherent catalytic performance metric of the two metals (i.e., ruthenium and nickel) in terms of the reductive amination reaction applied to bio-derived molecules. At the same time, all controllable variables have been kept identical at every stage, including the support material followed by tuning of these parameters to maximize the reaction yields and conversion. We report the catalytic performance comparison in terms of reaction yield, reaction time, required metal composition in the catalyst, reaction temperature, and pressures between ruthenium and nickel on MMT-K10 clay in varying amounts towards the reductive amination of biomass-derived as well as other aryl molecules to corresponding primary amines. Similarly, reductive amination of crude furfural extracted from xylose and lignocellulosic biomass hydrolysis has also been explored using both Ru and Ni-nanocomposites.

Experimental

Materials

Furfural (>98%), 5-hydroxymethyl furfural (HMF) (>98%), 5-methyl furfural (>97%), 4,5-dimethyl furfural (>97%), and other phenyl aldehyde substrates were purchased from Sigma Aldrich, India, and Alfa Aesar, India. MMT-K10 clay was purchased from Sigma Aldrich, India. Nickel sulfate hexahydrate ($NiSO_4$. $6H_2O$) (98%) was acquired from Alfa Aesar, India. Ruthenium chloride ($RuCl_3$. xH_2O) and Sodium borohydride ($NaBH_4$) was purchased from Sigma Aldrich, India. Ammonia aq. solution (25%) was purchased from Sigma Aldrich, India. All solvents (AR grade) were obtained from Alfa Aesar, India.

Catalyst synthesis

The nanocomposites were synthesized using a known procedure with minor modifications [33,34]. Ruthenium loaded nanocomposites were synthesized with 1%, 2%, 3%, 4% wt. metal loading percentage, with respect to the MMT clay support. Nickel nanocomposites utilized 10%, 12.5%, and 15% metal loading percentages for the reaction under focus. The procedure for synthesis was as follows: 100 mL of Milli-Q water was charged into a three-neck round bottom flask. 1 g Na-MMT was added to the flask, and the flask was sonicated for 30 min. Corresponding metal salt ($RuCl_3$ .x H_2O or $NiSO_4$. $6H_2O$) was weighed according to desired weight loading and transferred to a 250 mL beaker. Then the salt was dissolved in 150 mL of Milli-Q water. Then the metal salt solution was transferred to the three-neck flask. This solution was then subjected to 1 h of N_2 gas bubbling to remove any dissolved oxygen with vigorous stirring. 5 equivalents of $NaBH_4$ were weighed separately and then dissolved in 100 mL of Milli-Q water. This reducing solution was then added dropwise to the suspended stirring solution in the three-neck flask with continued N_2 bubbling of nitrogen over a period of 30 min. The resultant black material was separated by decantation and washed once with Milli-Q water and twice with acetone. The material was dried at room temperature in a desiccator for 24 h. The prepared and dried nanocomposites with ruthenium and nickel were calcined at 170 °C and 500 °C respectively with 80:20 ratio of N_2:H_2 gaseous mixture for three hours each in a tube furnace. The respective reduction temperatures were determined from H_2-TPR analysis for both the nanocomposites.

General procedure

The general procedure for the reductive amination reactions involves the use of a 100 ml capacity autoclave at 400 rpm. The optimized reaction conditions for Ru- based nanocomposite are as follows: 90 °C, 0.5 mmol of the aldehyde, 4 ml of 25% ammonia solution, 30 mg catalyst, 10 bar H_2 pressure. While the Ni-based nanocomposite employed reaction conditions as: 130 °C, 0.5 mmol of aldehyde, 4 mL of 25% ammonia solution, 30 mg catalyst, 15 bar H_2 pressure. After the reaction, the reaction mixture was centrifuged and filtered to separate the catalyst. The solvent from the reaction mixture was removed on rotary evaporator. The dense residual liquid was then dissolved in ethyl acetate and passed through sodium sulfate bed for removing residual moisture. Further purification of the product was carried out by column chromatography using neutral alumina with PET ether/ethyl acetate system.

Results and discussion

Various characterization techniques were employed to analyze distinctions between the respective nanocomposites. The techniques utilized includes P-XRD, XPS, SEM-EDX, BET surface area analysis, NH_3-TPD, H_2-TPR, Py-IR, HR-TEM. X-ray diffraction studies were conducted to identify the metal by characteristic peaks as well as verify the nanoscale of metal crystallite in the nanocomposite. Diffraction spectra stack has been shown in Fig. 1A and B. Representative peaks of montmorillonite K10 clay appear at $2\theta = 5.19°$, 20.81°, 26.65°, 34.98°, 45.55°, and 61.75°. The representative ruthenium nanoparticle peaks appear at $2\theta = 43.98°$ and 78.6°, which match the ICDD-JCPDS card number: 6-0663 for ruthenium metal, matching with the (101) and (103) mirror planes respectively [35]. The low intensity of the characteristic ruthenium nanoparticle peaks can be owed to the sub-4% loading on the support material. Average crystallite size determined using Scherrer's equation in reference to the highest intensity peak at 43.98° was found to be in the range of 10–12 nm.

Around $2\theta = 5.14°$, the peak in Fig. 1B, which depletes in intensity considerably, after subsequent loading of Ni metal on the support material, signifies the exfoliation of the ordered lamellar structure of the K10-clay resulting in increased surface area and porosity. The same effect is not observed in the 2% Ru/MMT as the percent loading of ruthenium is significantly lower than the nickel nanocomposite. The pre-calcined nanocomposite peaks do not demonstrate peaks relative to the β-Ni, unlike the calcined material. This emphasizes the amorphous nature of the material prior to the calcination step. The calcined material, however, shows the definitive characteristic peaks of the Ni crystallite structure at $2\theta = 44.29°$, 51.77° and 76.40°, [36] in good agreement with the ICDD-JCPDS card number: 01-071-4655. The average crystallite size of the Ni nanoparticles was calculated using Scherrer's equation with the highest intensity peak at 44.29°, which was found to be in the range of 18–20 nm. The remainder peaks of MMT clay have been highlighted in Fig. 1A and B. There is a negligible presence of NiO in the material post calcination with respect to the diffraction data. XPS measurements were further employed to confirm and determine the Ru and Ni oxidation states in the structured nanocomposite of 2% Ru/MMT and 12.5% Ni/MMT in Fig. 1C and D. The peaks corresponding to the $3d_{3/2}$ and $3d_{5/2}$ at 284.8 eV and 280.1 eV ascertain the presence of

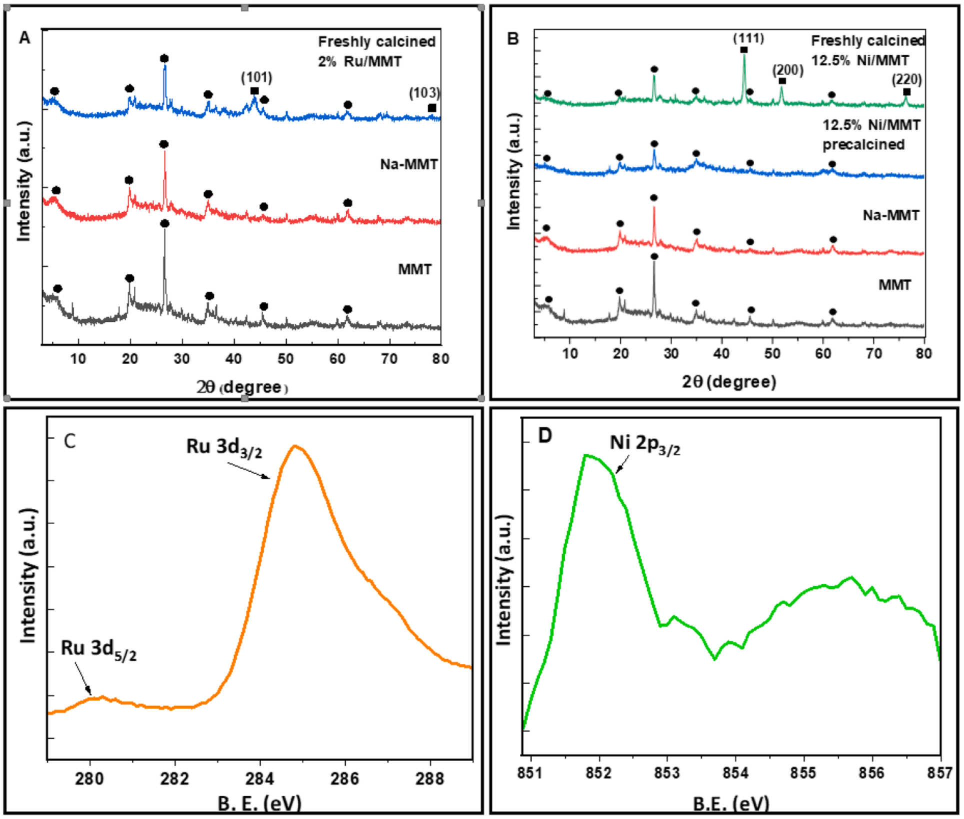

Fig. 1. (A) PXRD stack for MMT k10, Na-MMT and 2% Ru/MMT (B) PXRD stack for MMT k10, Na-MMT, pre-calcined 12.5% Ni/MMT and Fresh calcined 12.5% Ni/MMT (Circle dots define representative peaks for MMT and square dots define corresponding peaks for ruthenium and nickel in each stack) (C) Ru 3d region of 2% Ru/MMT (D) Ni 2p region of 12.5% Ni/MMT.

Ru in the metallic state in the 2% Ru/MMT nanocomposite. The broad nature of the peaks in the Ru $3d_{5/2}$ spectra do suggest the presence of RuO_2, but it is almost negligible in concentration. The survey spectra for both the nanocomposites have been presented in the ESI (Figure S3 and S4). The Ni 2p spectra of fresh 12.5% Ni/MMT shows a large peak at 851.99 eV, which signifies the nickel on the surface of the material in the metallic state. There is the appearance of satellite peaks in the range of 854–856 eV, implying the presence of Ni in the NiO state as well. Moreover, there appears to be a 1 eV shift to larger binding energy in the Ni 2p spectra, which can be due to the strong bonding of the metallic nanoparticles to the support material lattice signifying intercalation to a certain degree [34].

HR-TEM imaging showed the particle size to be in the range of 20–25 nm for both 2% Ru/MMT and 12.5% Ni/MMT in Fig. 2. A and D.

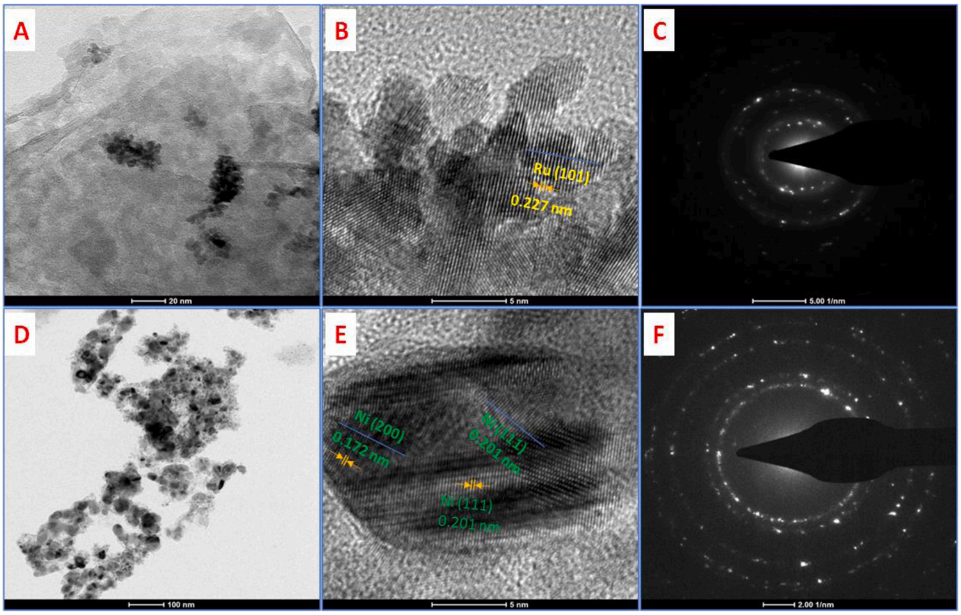

Fig. 2. HR-TEM imaging and SAED analysis of A, B & C] 2% Ru/MMT D, E & F] 12.5% Ni/MMT.

The TEM imaging of 12.5% Ni/MMT showed uniform distribution of nickel nanoparticles. The high-resolution images show the Ru (101) matching with the fringe width of 0.227 nm for 2% Ru/MMT. As for 12.5% Ni/MMT, Ni (111) and Ni (200) planes are shown in Fig. 2. E in a nickel nanoparticle. The SAED analysis showed a polycrystalline structure of the metallic nanoparticles (i.e., Ru and Ni) with the crystalline support material, MMT clay, with multiple planes. Scanning Electron Microscopy- Energy Dispersive X-ray Spectroscopy (SEM-EDX) technique was required to analyze the morphology and the elemental mappings to get the dispersion of the metals on the surface of the material in Fig. 3. A-E. The images in Fig. 3. A and C show the exfoliated lamellar layers of the MMT support for both the ruthenium and nickel-based nanocomposite respectively with distinct cracks and folds around the edges of the material, exposing the inner sheets of the material. The elemental mappings of 2% Ru/MMT and 12.5% Ni/MMT are shown in Fig. 3. B and D, suggesting uniform and fine dispersion of ruthenium (green dotting) and nickel (white dotting) among the surface of both catalysts respectively. The additional elemental mappings and EDX spectra have been added to the ESI (Figure S5–S8).

BET surface area has also been calculated to exhibit the surface area, pore volume, and diameter distinctions after loading of ruthenium and nickel metal forming the respective nanocomposites (Table 1). The parameters such as BET surface area and pore diameter offers significant insights into the difference in the catalytic performance of these two nanocomposites for the reductive amination reaction. The surface acidity analyses were conducted using techniques such as NH_3-TPD, H_2-TPR, Py-IR spectroscopy [37,38]. NH_3-TPD analysis was carried out to provide the strength of acidic sites in both the nanocomposites, which is vital for their catalytic performance in Fig. 4. While both the catalysts displayed distinctly weak (100–250 °C) to moderate acidic sites (350–450 °C) from the analysis (Fig. 4), the TCD signal around 350–500 °C was much lower for 12.5% Ni/MMT as compared to 2% Ru/MMT, which signifies the smaller number of moderate strength acidic sites in 12.5% Ni/MMT [39,40]. This factor plays an influential role in the difference between the catalytic performance of these nanocomposites for the reductive amination reaction. The details about the Brønsted and Lewis acidic sites for both catalysts were shown by Pyridine adsorption Infrared Spectroscopy (Py-IR) (Figure S10). The Brønsted acidic sites absorbance appeared at 1541 cm^{-1} (pyridinium ion stretch), while peak around 1446 cm^{-1} and 1590 cm^{-1} account for the Lewis acidic sites [41]. As the metal loading in case of 2% Ru/MMT is lower than the Ni nanocomposite, the Brønsted acid site absorption at 1541 cm^{-1} is much preeminent than 12.5% Ni/MMT. Moreover, the intensity of Brønsted acid and Lewis acid sites are mostly equal in case of 2% Ru/MMT but Lewis acid sites dominate in case of 12.5% Ni/MMT. The combination peak of both kind of sites appears at 1490 cm^{-1}, has higher intensity in case of Ru nanocomposite. However, the Lewis acid site absorption at 1446 cm^{-1} and 1590 cm^{-1} is much higher for 12.5% Ni/MMT as the higher metal loading greatly amplified the quantity of these sites. As more metal loading reduces the Brønsted acid sites on the surface, new acid sites are formed on the MMT surface. The peak at 1635 cm^{-1} is the vibration peak of the adsorbed moisture on the catalyst surface. H_2-TPR studies were conducted to deduce the reduction temperatures of the respective metals in Fig. 4. B, 2% Ru/MMT shows an intense peak at 146 °C exhibiting the reduction of finely dispersed RuO_2 to Ru metal and the high temperature peak at 545 °C in 2% Ru/MMT corresponds to the reduction of oxidized Ru species with strong interactions with the support surface [42]. As for 12.5% Ni/MMT, an intense broad peak could be observed with apex points at 467 °C [reduction of NiO to Ni (0) species] and at 519 °C that could be accounted for the reduction of Ni species having stronger interaction with the MMT surface [39].

Table 1
BET surface analysis data for Ru and Ni-based nanocomposites.

Sr. No.	Catalyst	BET surface area ($m^2\ g^{-1}$)	Pore volume ($cm^3\ g^{-1}$)	Average pore diameter (Å)
1	2% Ru/MMT	155.4	0.42	108.23
2	12.5% Ni/MMT	122.9	0.26	86.14

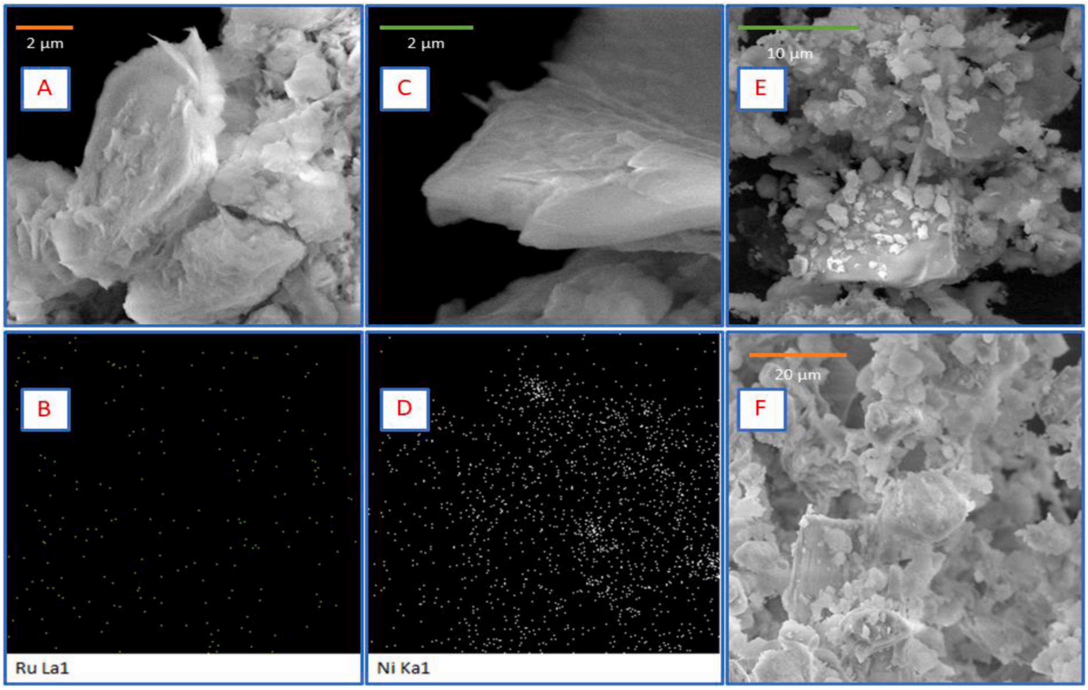

Fig. 3. A and B] SEM image and Elemental mapping for 2% Ru/MMT
C and D] SEM image and Elemental mapping for 12.5% Ni/MMT E] SEM-EDX image for 12.5% Ni/MMT
F] SEM-EDX image for 2% Ru/MMT.

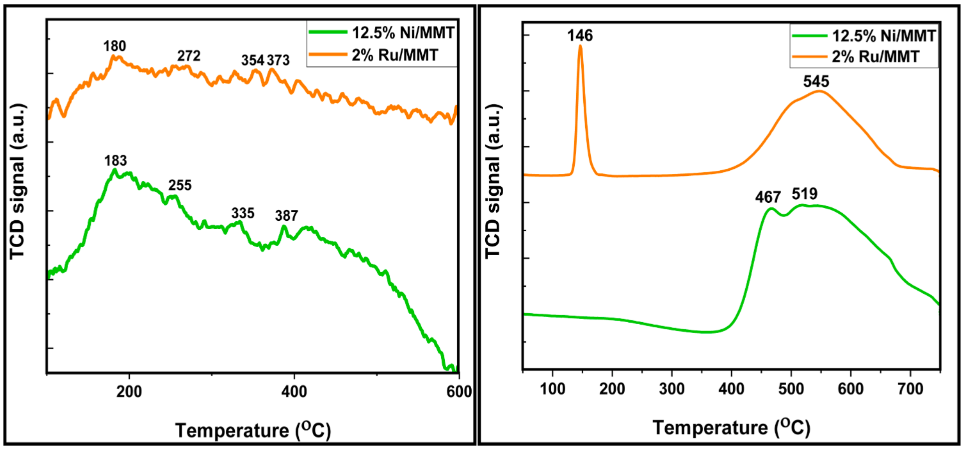

Fig. 4. (A) NH_3-TPD profile for both catalysts B) H_2-TPR profile for both catalysts.

Activity studies

The process optimization for both the ruthenium and nickel-based nanocomposites includes the synthesis of a library of primary amines using commercially available liquor ammonia (25% aq. solution) and molecular hydrogen. The reaction scheme and the preliminary reaction parameters are shown in Table 2. Various composition catalysts were tested in identical conditions to determine the optimal metal loading percentage for both the metallic nanocomposites. Furthermore, various parameters were optimized, with the goal of maximizing the yield that includes reaction temperature, hydrogen pressure, catalyst amount, reaction time, and ammonia concentration. As for the Ru particle size correlation with catalytic performance, the average crystallite sizes were calculated by Scherrer's equation for all synthesized ruthenium nanocomposites. The respective XRD spectra stack for 1%, 2%, 3% and 4% Ru/MMT nanocomposites has been included in the ESI (Figure S9). The preliminary reaction conditions have been mentioned in Table 2 Preliminary scheme 1. These conditions produced 71% of furfuryl amine 1 (a), with 21% of 2-furanmethanol 1(b) as well as 11% of 1(c) of secondary amine by-products in the case of 4% Ru/MMT (Average crystallite size of Ru= 12.9 nm). While 15% Ni/MMT catalyst exhibited 62% selectivity towards the desired primary amine product. 12.5% Ni/MMT yielded selectivity of 1 (a) comparable to 2% Ru/MMT at 63% (average crystallite size=10.8 nm). The respective metal percentages have been highlighted in Table 2. Moreover, the selectivity values for Ru-nanocomposites in Table 2 do match with previously reported observations, [43] which shows higher reduction product [1(b)] selectivity with increasing Ru particle size. The selectivity of 1(a) was not affected much at higher Ru loading percentages, however it dropped going from 2% (68%) to 1% Ru/MMT (58%) with reduced conversion. Henceforth, the most optimal catalytic systems were found to be 2% Ru/MMT and 12.5% Ni/MMT with respect to maximizing yield and selectivity of 1(a). These nanocomposites were further investigated for optimizing the reaction process. Different parameters were tested to tune the reaction to find the middle-point for best performance for both of the catalysts to present their comparison. 1(b) is the reduction by-product in the reductive amination process shown by the GC–MS analysis, while 1(c) being the reductive amination coupling of the primary amine to the unreacted furfural molecule forming the secondary amine.

Effect of temperature

For further improving yields and conversion, both the catalysts were tested at different temperature ranges from 80 to 140 °C in Fig. 5. A and B. All the other conditions were kept identical to the conditions mentioned in Scheme 1. At 130 °C, 12.5% Ni/MMT exhibited 63% selectivity of 1(a) in 7 h at 25 bar H_2 pressure. However, increasing the temperature to 140 °C does not effectively translate into higher yields, giving 64% selectivity of 1(a), but increasing selectivity towards 1(b) to 19%. Lowering the temperature from 140 to 80 °C reduced the overall% conversion of 1(a), (b) & (c). Thus, 130 °C was found to be the effective optimal temperature for the 12.5% Ni/MMT catalyst. 2% Ru/MMT showed a different trend with maintaining on par % conversion while increasing yield of 1(a) till 90 °C. However, as the temperature was

Table 2
Catalyst screening for reductive amination of bio-derived aldehydes.

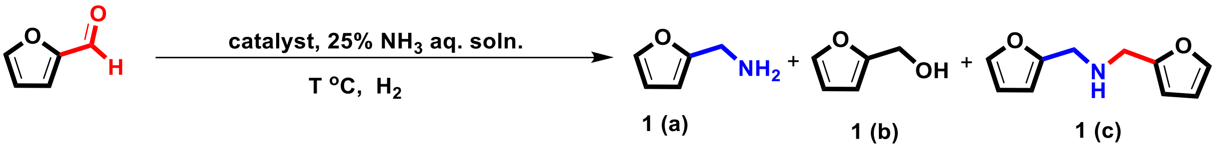

Preliminary Scheme 1[a]

Catalyst	% Conversion	(%) Selectivity[b]		
		1(a)	1(b)	1(c)
4% Ru/MMT	99	71	21	7
3% Ru/MMT	97	68	22	10
2% Ru/MMT	98	68	14	12
1% Ru/MMT	91	58	11	6
15% Ni/MMT	93	62	18	13
12.5% Ni/MMT	91	63	15	8
10% Ni/MMT	89	54	16	9

[a] Preliminary reaction conditions: 0.5 mmol reactant, 30 mg catalyst, 2 mL 25% NH_3 aq. soln., 130 °C, 25 bar H_2 pressure, 7 h.
[b]Confirmed & Calculated by GC & GC–MS (%).

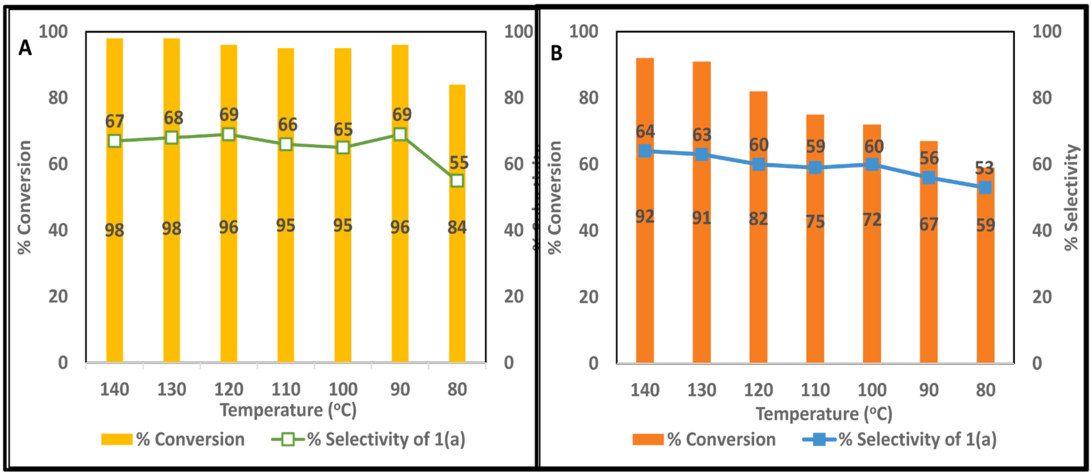

Fig. 5. Effect of Temperature (A) 2% Ru/MMT B) 12.5% Ni/MMT.
Reaction conditions of A & B: 0.5 mmol reactant, 30 mg catalyst, 25 bar H_2 pressure, 2 mL 25% NH_3 aq. soln., 7 h.

reduced to 80 °C, the% conversion reduced significantly from 96% to 84%. Thus, 90 °C was used for further activity studies for 2% Ru/MMT.

Effect of hydrogen pressure

Parameters such as hydrogen pressure play a huge role in reductive amination reactions as they aid in tuning the selectivity of the catalyst towards reduction-only products and reductively aminated ones. In this work, we analyzed reaction runs from a range of 25 bar to 5 bar H_2 pressure. However, testing the pressure beyond 25 bar was not much of a consequence as the desired selectivity was not achievable at higher hydrogen pressures. In Fig. 6. A and B, it can be observed that as the pressure is lowered, the selectivity of 1(a) increased significantly, which may be due to reduced adsorption of H_2 molecules at lower pressures leaving more vacant active sites for ammonia molecules to be adsorbed. The reductive amination reaction requires a competitive adsorption process between ammonia and hydrogen molecule, which steers the selectivity towards amination or reduction products. The highest selectivity of 82% was achieved over 10 bar of H_2 pressure at 90 °C with 2% Ru/MMT catalyst. Nickel catalyst produced the highest of 78% selectivity at 15 bar H_2 pressure at 130 °C. The sudden decrease in conversion for the 12.5% Ni/MMT may be explained by the lower adsorption efficiency of H_2 molecules on catalyst surface at lower pressures leading to incomplete conversion of reactant.

Effect of ammonia concentration

As mentioned, the reductive amination reaction requires two competing processes of amination and hydrogen reduction on the catalyst surface. The dominating species in these two directs the selectivity for the reaction. Thus, optimal ammonia concentration is key to prioritizing the primary amine products over other by-products. In this case, the graphs in Fig. 7A and B effectively show the changes in conversion and selectivity to that of the substrate to ammonia mole ratio. Both the Ru and Ni- nanocomposites were found to require the 50:1 ratio of ammonia to substrate respectively, to obtain maximum selectivity towards the synthesis of furfuryl amine. Between the range of 2 mL to 5 mL, 4 mL of 25% NH_3 solution (substrate/ammonia mole ratio = 0.01) was determined to be the ideal ammonia concentration for the process.

Effect of duration

The graphs in Fig. 8. A and B show the reaction time optimization for Ru and Ni-nanocomposites. 2% Ru/MMT showed the highest selectivity of 1 (a) at 96% in 3 h. The selectivity decreased by slight amounts at higher time periods. It can be explained by coupling of unreacted furfural with furfuryl amine [1(a)] to form corresponding imine or secondary amine as the 1(c) by-product in smaller steady increments. This type of observation was also observed by Maya et.al. [22], where

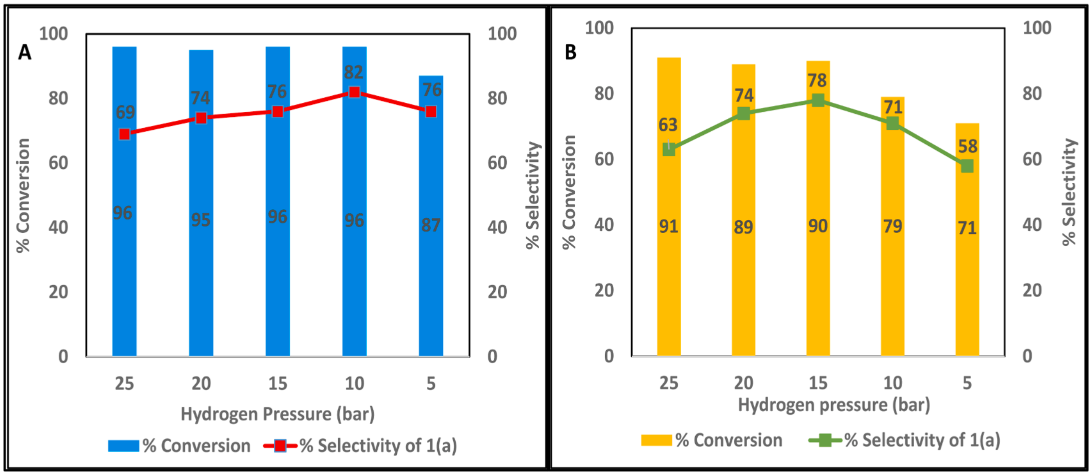

Fig. 6. Effect of H_2 pressure A) 2% Ru/MMT B) 12.5% Ni/MMT.
Reaction conditions of A (Temp. 90 °C) & B (Temp. 130 °C): 0.5 mmol reactant, 30 mg catalyst, 2 mL 25% NH_3 aq. soln., 7 h.

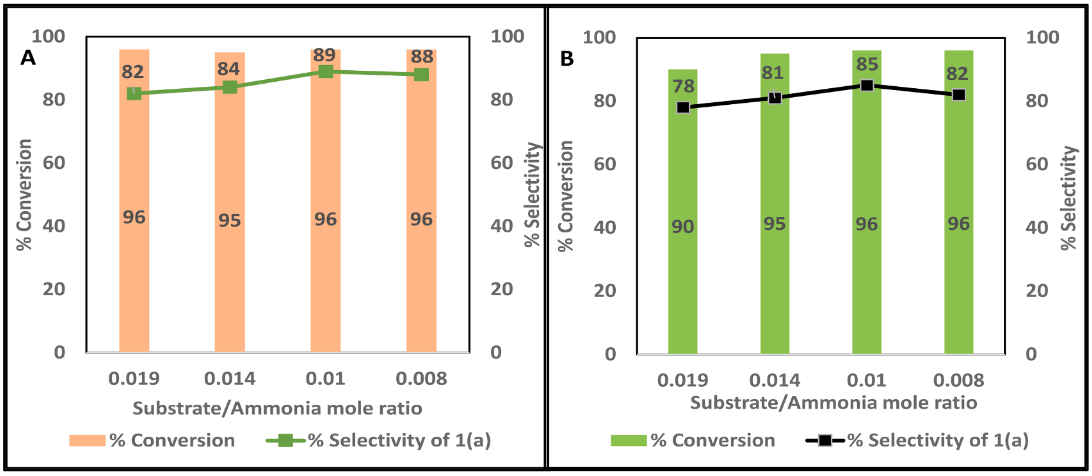

Fig. 7. Effect of ammonia concentration A) 2% Ru/MMT B) 12.5% Ni/MMT.
Reaction conditions of A (90 °C, 10 bar H_2 pressure) & B (130 °C, 15 bar H_2 pressure): 0.5 mmol reactant, 30 mg catalyst, 7 h.

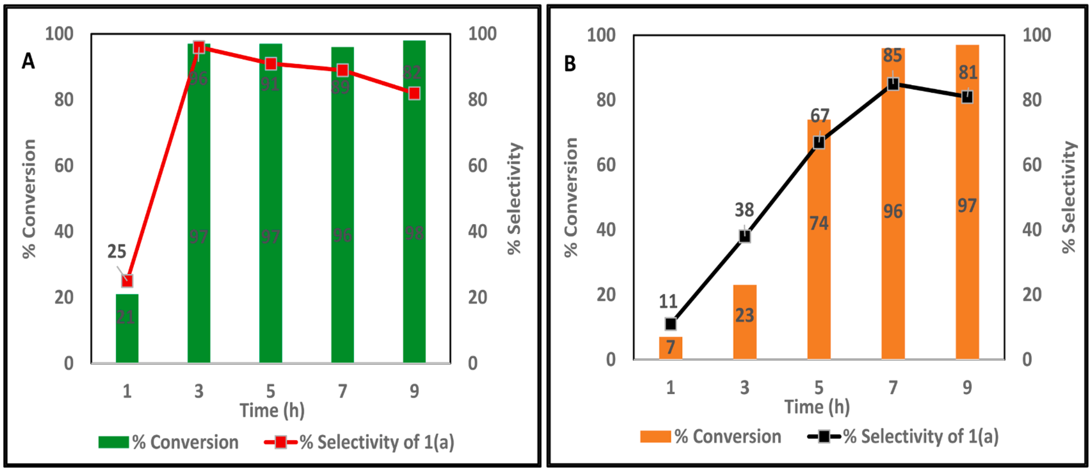

Fig. 8. Effect of Duration A) 2% Ru/MMT B) 12.5% Ni/MMT.
Reaction conditions of A (90 °C, 10 bar H_2 pressure) & B (130 °C, 15 bar H_2 pressure): 0.5 mmol reactant, 30 mg catalyst, 4 mL 25% NH_3 aq. soln.

the secondary amine selectivity steadily increased although by minor percentages in similar effect. In this case, the selectivity of the reduction by-product 1(b) rose as well but stayed relatively constant after 5 h of reaction time for 2% Ru/MMT. Whereas, 12.5% Ni/MMT followed a similar trend in terms of selectivity on the selected timescale for this process. There have been reports where secondary amines have been produced by using the same catalysts, [25,27] being used for synthesis of primary amines. The secondary amine selectivity of 2% Ru/MMT and 12.5% Ni/MMT is much lower (~5–10%) signifying the high selectivity of these nanocomposites for the synthesis of primary amines at these reaction parameters. 12.5% Ni/MMT catalyst runs observe a different trend with the highest selectivity achieved at 7 h with 85% selectivity of 1(a). Additionally, 12.5% Ni/MMT also observes a considerable increase in% conversion over time and reaches a maximum at 96% in 7 h of the run.

Substrate scope

Both these catalysts were further assessed for their catalytic ability with different heterocyclic, bio-derived, and aryl aldehydes at their optimized process conditions in Table 3. The biomass-derived molecules such as 5-hydroxymethyl furfural gave appreciable yields with both 2% Ru/MMT and 12.5% Ni/MMT catalysts at 86 and 79%, respectively (Table 3 Entry 2). 5-methyl furfural substrate gave a decent yield of 83% and 76% with both Ru and Ni catalyst respectively, while previous reports include Ru/ZrO_2 (61%), [23] Rh/Al_2O_3 (91% selectivity), [22] and Ru-NPs (68%) [22]. The relative lower yields with previous catalysts may be due to the property of 5-methyl fufural to form a dimer by air oxidation. Hence, it requires inert atmosphere operation till addition to the batch autoclave to maximize the yields. From Table 3 Entry 2, the reaction times for all the substrates were increased to 6 h and 10 h for 2% Ru/MMT and 12.5% Ni/MMT respectively, to achieve maximum conversion for all remaining substrates. While other commercially available furfural derivatives were also tested, which includes 4, 5-dimethyl furfural gave an excellent yield of 91% with 2% Ru/MMT, being the highest yield reported yet (Table 3 Entry 4). The highest reported selectivity for this product has been ~61% with presence of mixture of reduction and coupling products. [22] Heterocyclic aldehyde was also tested to show the scope of these catalysts with 2-thiophene carboxaldehyde substrate producing yields in the range of 64 and 77% with both the catalysts (Table 3 Entry 5), which is higher than previously reported yields (~57%) by Komanoya *et.al* using Ru/Nb_2O_5. [24] Other aryl aldehydes with different functional groups were also used for this library, which gave decent yields on both catalysts with complete conversions. Halogenated aldehydes are usually most unreliable in terms of reactivity, leading to many issues such as dehalogenation of the

Table 3
Substrate based catalyst performance comparison.

Entry No.	Reactant	Product	2% Ru/MMT[a, c]		12.5% Ni/MMT[b, c]	
			Time (h)	(%) Conv./ Yield	Time (h)	(%) Conv./ Yield
1	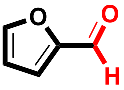	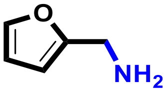	3	97 / 89	7	96 / 84
2	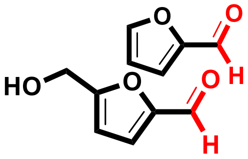	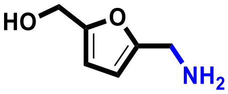	3	98 / 86	7	94 / 79
3	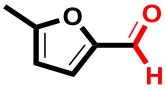	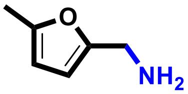	6	98 / 83	10	93 / 76
4	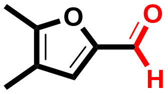	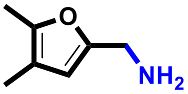	6	96 / 91	10	98 / 83
5[d]	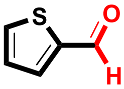	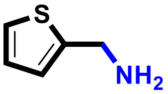	6	99 / 77	10	93 / 64
6	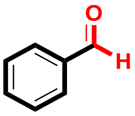	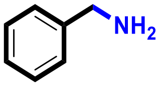	6	100 / 89	10	100 / 72
7	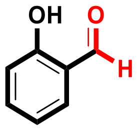	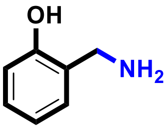	6	100 / 85	10	98 / 67
8[d]	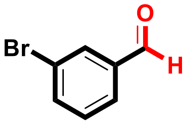	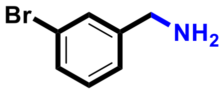	6	100 / 92	10	95 / 61
9[d]	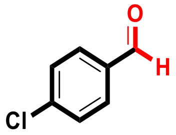	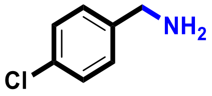	6	100 / 96	10	91 / 69
10[d]	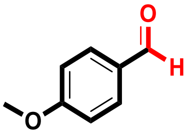	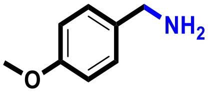	6	100 / 91	10	95 / 83
11[d]	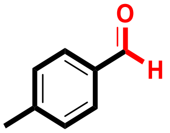	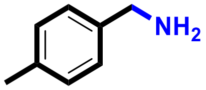	6	100 / 93	10	91 / 86

[a] Optimised reaction conditions: 30 mg catalyst, 90 °C, 10 bar H_2 pressure, 0.5 mmol reactant, 4 mL 25% NH_3 aq. soln.
[b] Optimised reaction conditions: 30 mg catalyst, 130 °C, 15 bar H_2 pressure, 0.5 mmol reactant, 4 mL 25% NH_3 aq. soln.
[c] GC & GC–MS yield% [d] 3 mL EtOH was added to mixture.

substrate, low conversions requiring harsher reaction parameters to achieve conversion. However, 2% Ru/MMT exhibited exceptional performance with 96% for the 4-chloro substituted substrate at the same reaction conditions (Table 3 Entry 9), which is comparable to Ni_6AlO_x (81%) [27] and Ru-NPs (90%) [26]. Salicylaldehyde as a substrate showed 100% conversion with 85% and 67% yield with 2% Ru/MMT and 12.5% Ni/MMT respectively (Table 3 Entry 7), which is the highest yield achieved with no recent reports for this substrate. Additionally, 3-Bromo benzaldehyde reaction showed yields of 92% and 61% with the Ru- and Ni-based nanocomposites respectively, which are akin to reported para-substituted substrates with Br (91%) and Cl (90%) functionality using ruthenium templated nanoparticles [26]. Ortho and meta substituted substrates reactions were demonstrated to showcase the excellent functional group and electronic effect tolerance of these catalysts for the reductive amination reaction. 4-Anisaldehyde substrate reaction resulted in a yield of 91% and 83% for 2% Ru/MMT and 12.5% Ni/MMT respectively (Table 3 Entry 10). 4-Tolualdehyde reaction produces similar results with yields in the range of 93–86% for both the nanocomposites (Table 3 Entry 11). ^{1}H, ^{13}C NMR, and GC–MS of the selected compounds have been added to the ESI (Fig. S11-S25).

Reusability and control experiments

The recyclability of these nanocomposites was also tested by reusing the catalyst over 5 more recycle runs after the fresh catalyst run in Fig. 9. The reaction runs utilized parameters as optimized in the prior stage of the study. After each run, the reaction mixture was centrifuged at 10,000 rpm and the catalyst was separated from the reaction mixture. The Ru catalyst was washed twice with methanol and then dried at 55 °C. However, the Ni catalyst was washed twice with acetone and dried in a vacuum desiccator at 40 °C. The 2% Ru/MMT shows excellent yields of 1(a) up to the 5th recycle ranging from 95% to 90%. As for 12.5% Ni/MMT, the yields effectively reduced below 80% at the 3rd recycle run at 75%. There may be two factors contributing to this with a higher rate of oxidation of surface Ni (0) species on MMT surface compared to Ru metal. The X-ray diffraction spectra of recycled catalysts show agglomeration of nanoparticles up to a certain extent in the form of broader characteristic peaks in the ESI (Figure S1 and S2). The control experiments were conducted in multiple different scenarios in the absence of a catalyst (Table S1 Entry 1), with just MMT without metal loading (Table S1 Entry 2), with and without ammonia or hydrogen pressure for both nano-composites (Table S1 Entry 3–6). Trace amounts of 1(b) were detected in the base MMT run (Table S1 Entry 2). Absence of aq. ammonia run (Table S1 Entry 3–4) yielded 22% and 29% of 1(b) for 2% Ru/MMT and 12.5% Ni/MMT respectively. All controlled reaction runs showed zero presence of 1 (a), showing the requirement for each of the optimized parameters of the reaction. These experiment runs also demonstrate a clear reaction pathway for conversion of aldehydes into their primary amine products. The reaction in presence of MMT (30 mg) yielded trace presence of the 1(b) reduction by-product. This shows the ability of the laminar alumino silicate structure to adsorb hydrogen molecules on its Brønsted acidic active sites, increasing the density of hydrogen molecules in the vicinity of the catalyst surface. [42] While, the Ru/MMT and Ni/MMT catalyst runs in absence of aq. ammonia produced 1(b) in higher quantities showing that reduction step is carried out more efficiently in presence of the metallic nanoparticles. Moreover, the no aq.ammonia and no hydrogen pressure runs elucidate the reaction pathway, in which the aldehyde and ammonia molecule couple together by hydrolysis forming an imine, the reversible reaction intermediate [24]. This molecule further reacts at the Ru or Ni active sites with hydrogen to form the respective primary amine. Side reactions involve reduction of the aldehyde at the active sites to form the alcohol by-product.

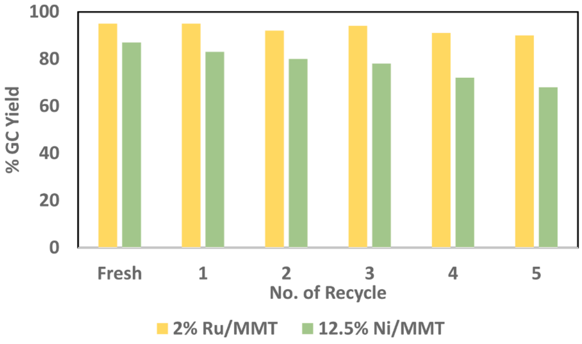

Fig. 9. Recyclability analysis of nanocomposites.

Reaction using crude biomass derived furfural

These catalytic nanocomposites were further used for reductive amination procedure with crude furfural as the substrate extracted from two sources, namely xylose [44] and lignocellulosic biomass feedstock (rice husk) [45] in Fig. 10. The xylose dehydration and biomass hydrolysis process yielded a dark brown-yellow liquid obtained after removing the solvent for both the extracts, which was used further without purification for the reductive amination step. The xylose extract substrate (100 mg) reaction gave a yield of 36% and 23% with the optimized reaction conditions with 2% Ru/MMT and 12.5% Ni/MMT respectively (Table 4). In contrast, the biomass hydrolysis extract reaction exhibited a yield of 21% and 11% for 2% Ru/MMT and 12.5 Ni/MMT respectively. The yields are much lower than expected for both the 2% Ru/MMT and 12.5% Ni/MMT catalyst for this reaction. It may be due to two factors affecting the yields, which are: a) Firstly, low conversion and yields due to high amount of impurities present in the derived furfural extract from both sources(especially higher in the rice husk extract) resulting in high impurity intolerance of these catalysts. b) Secondly, it may be due to side reactions of synthesized furfurylamine with the other impurities having varying functional groups. Although, 2% Ru/MMT showed much better catalytic yields in comparison to 12.5% Ni/MMT for the same process by factor of ~1.5–2. As the ruthenium nanocomposite showed encouraging results in terms of reductive amination reaction in terms of yield and selectivity, hence we have assessed the industrial scalability of the 2% Ru/MMT nanocomposite as a catalyst for conversion of furfural to furfuryl amine. The gram scale run for the reductive amination of furfural with 2% Ru/MMT in a batch autoclave gave a yield of 69% at 20 bar H_2 pressure, 120 °C, 14 h, shown in Fig. 11. We employed harsher conditions for the gram scale reaction with higher amount of bulk reactants (hydrogen and ammonia). However, we employed lower than extrapolated quantity of 2% Ru/MMT (~100 mg) yet it exhibited decent conversion and good yield . Higher temperature was applied to increase the rate of the reaction to reduce the time factor. While, the concentrations of hydrogen gas and ammonia were scaled according to the furfural concentration. The Ru based nanocomposite with montmorillonite clay is a versatile material as it has impressive catalytic activity for reductive amination reaction. The reusability studies also showed no significant change in activity over multiple cycles signifying the *in-situ* regeneration of Ru (0) in the material requiring no need for separate regeneration or calcination step. The Ni nanocomposite on the other hand may require the calcination step as based on the H_2-TPR analysis, the temperature essential for reduction of Ni species on the support surface is much higher than the Ru counterpart. Additionally, NH_3-TPD analysis showed presence of weak as well as moderate strength acidic sites, which when correlated with the difference in activity of the Ru and Ni based nanocomposite. Based on the activity results, It is apparent that the presence of these relatively higher number of stronger acidic sites (350–450 °C) contributes heavily to their catalytic role in the reductive amination process for the Ru-based nanocomposite. This data also correlates well with the Py-IR absorption spectra of both the nanocomposites where equal quantities of these sites in 2% Ru/MMT greatly enhance the yield as well as the catalytic performance. However, an imbalance of these sites in 12.5% Ni/MMT requires harsher conditions to perform at an equivalent level. This shows the requirement of balanced quantitites of both Brønsted and Lewis acid sites for the reductive amination reaction.

Conclusion

This work demonstrated the catalytic comparison of MMT supported ruthenium and nickel nanoparticles for the reductive amination of bio-

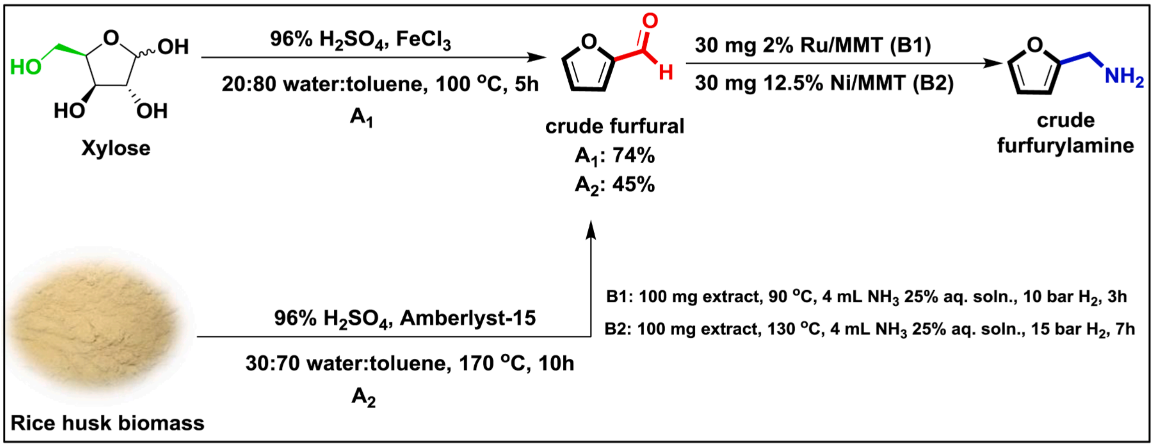

Fig. 10. Reductive amination process for crude extracted furfural.

Table 4
Reductive amination of crude bio-derived furfural extracts.

Process	2% Ru/MMT B1 (%)[a,b]	12.5% Ni/MMT B2 (%)[a,b]
Xylose extract	36	23
Biomass extract	21	11

[a] GC yield (%).

[b] confirmed by GC–MS

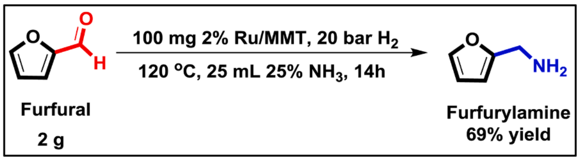

Fig. 11. Gram scale reductive amination of furfural.

derived and other aryl aldehydes. Montmorillonite as an inexpensive support material clearly exhibits decent to exceptional performance in this process, for a wide substrate scope. Ru/MMT provides better catalytic performance relative to Ni/MMT in terms of required metal loading, reaction conditions, primary amine selectivity and reusability. However, Ni/MMT has been shown to achieve on par catalytic performance by adopting slightly harsher reaction conditions. The two metallic nanocomposites also scale agreeably with a wider substrate scope, including varied aryl and heterocyclic aldehydes. Moreover, these nanocomposites showed decent performance in converting crude furfural extracted from xylose dehydration and biomass hydrolysis (rice husk) to the primary amine counterpart. Additionally, the gram scale conversion using 2% Ru/MMT nanocomposite exhibited encouraging results for the reductive amination of furfural.

CRediT author statement

Comparative account of catalytic activity of Ru- and Ni-based nanocomposites towards reductive amination of biomass derived molecules

Tejas A. Gokhale: Conceptualization, Methodology, Formal analysis, Validation, Investigation, Writing - Original Draft, Visualization.

Amol B. Raut: Conceptualization, Formal analysis, Writing - Review & Editing, Visualization

Prof. Bhalchandra M. Bhanage: Conceptualization, Methodology, Validation, Resources, Data Curation, Writing - Review & Editing, Visualization, Supervision, Project administration, Funding acquisition

Declaration of Competing Interest

The authors declare that they have no known competing financial interests or personal relationships that could have appeared to influence the work reported in this paper.

Acknowledgments

T.A.G. is grateful for research funding from the Department of Science & Technology, New Delhi, Government of India, under the DST-BRICS-ICP-BIO research project under DST/IMRCD/BRICS/PilotCall2/ICP-BIO /2018 (G). T.A.G. is also thankful to Dr. Sachin Sakate for timely provided Py-IR absorption analysis.

Supplementary materials

Supplementary material associated with this article can be found, in the online version, at doi:10.1016/j.mcat.2021.111667.

References

[1] M. Dusselier, M. Mascal, B.F. Sels, Top chemical opportunities from carbohydrate biomass: a chemist's view of the biorefinery, in: 2014: pp. 1–40. https://doi.org/10.1007/128_2014_544.
[2] L. Shuai, M. Talebi Amiri, J.S. Luterbacher, The influence of interunit carbon-carbon linkages during lignin upgrading, Curr. Opin. Green Sustain. Chem. 2 (2016) 59–63, https://doi.org/10.1016/j.cogsc.2016.10.001.
[3] P. Sudarsanam, R. Zhong, S. Van den Bosch, S.M. Coman, V.I. Parvulescu, B.F. Sels, Functionalised heterogeneous catalysts for sustainable biomass valorisation, Chem. Soc. Rev. 47 (2018) 8349–8402, https://doi.org/10.1039/C8CS00410B.
[4] J.S. Luterbacher, D.M. Alonso, J.A. Dumesic, Targeted chemical upgrading of lignocellulosic biomass to platform molecules, Green Chem. 16 (2014) 4816–4838, https://doi.org/10.1039/C4GC01160K.
[5] M.J. Climent, A. Corma, S. Iborra, Conversion of biomass platform molecules into fuel additives and liquid hydrocarbon fuels, Green Chem. 16 (2014) 516, https://doi.org/10.1039/c3gc41492b.
[6] B. Saha, M.M. Abu-Omar, Advances in 5-hydroxymethylfurfural production from biomass in biphasic solvents, Green Chem. 16 (2014) 24–38, https://doi.org/10.1039/C3GC41324A.
[7] X. Li, P. Jia, T. Wang, Furfural: a promising platform compound for sustainable production of C 4 and C 5 chemicals, ACS Catal. 6 (2016) 7621–7640, https://doi.org/10.1021/acscatal.6b01838.
[8] L. Hu, L. Lin, Z. Wu, S. Zhou, S. Liu, Recent advances in catalytic transformation of biomass-derived 5-hydroxymethylfurfural into the innovative fuels and chemicals, Renew. Sustain. Energy Rev. 74 (2017) 230–257, https://doi.org/10.1016/j.rser.2017.02.042.
[9] F. Leroux, P. Jeschke, M. Schlosser, α-Fluorinated ethers, thioethers, and amines: anomerically biased species, Chem. Rev. 105 (2005) 827–856, https://doi.org/10.1021/cr040075b.
[10] C. Gunanathan, D. Milstein, Selective synthesis of primary amines directly from alcohols and ammonia, Angew. Chemie Int. Ed. 47 (2008) 8661–8664, https://doi.org/10.1002/anie.200803229.

[11] A. García-Ortiz, J.D. Vidal, M.J. Climent, P. Concepción, A. Corma, S. Iborra, Chemicals from biomass: selective synthesis of N-substituted furfuryl amines by the one-pot direct reductive amination of furanic aldehydes, ACS Sustain. Chem. Eng. 7 (2019) 6243–6250, https://doi.org/10.1021/acssuschemeng.8b06631.

[12] M. Nasrollahzadeh, Green synthesis and catalytic properties of palladium nanoparticles for the direct reductive amination of aldehydes and hydrogenation of unsaturated ketones, New J. Chem. 38 (2014) 5544–5550, https://doi.org/10.1039/C4NJ01440E.

[13] V.V. Karve, D.T. Sun, O. Trukhina, S. Yang, E. Oveisi, J. Luterbacher, W.L. Queen, Efficient reductive amination of HMF with well dispersed Pd nanoparticles immobilized in a porous MOF/polymer composite, Green Chem 22 (2020) 368–378, https://doi.org/10.1039/C9GC03140E.

[14] T. Stemmler, A.-.E. Surkus, M.-.M. Pohl, K. Junge, M. Beller, Iron-catalyzed synthesis of secondary amines: on the way to green reductive aminations, ChemSusChem 7 (2014) 3012–3016, https://doi.org/10.1002/cssc.201402413.

[15] Z. Xu, P. Yan, W. Xu, S. Jia, Z. Xia, B. Chung, Z.C. Zhang, Direct reductive amination of 5-hydroxymethylfurfural with primary/secondary amines via Ru-complex catalyzed hydrogenation, RSC Adv. 4 (2014) 59083–59087, https://doi.org/10.1039/C4RA10349A.

[16] A.B. Raut, V.S. Shende, T. Sasaki, B.M. Bhanage, Reductive amination of levulinic acid to N-substituted pyrrolidones over $RuCl_3$ metal ion anchored in ionic liquid immobilized on graphene oxide, J. Catal. 383 (2020) 206–214, https://doi.org/10.1016/j.jcat.2020.01.020.

[17] S. Pisiewicz, T. Stemmler, A.-.E. Surkus, K. Junge, M. Beller, Synthesis of amines by reductive amination of aldehydes and ketones using Co 3 O 4 /NGr@C catalyst, ChemCatChem 7 (2015) 62–64, https://doi.org/10.1002/cctc.201402527.

[18] J.D. Vidal, M.J. Climent, P. Concepcion, A. Corma, S. Iborra, M.J. Sabater, Chemicals from biomass: chemoselective reductive amination of ethyl levulinate with amines, ACS Catal. 5 (2015) 5812–5821, https://doi.org/10.1021/acscatal.5b01113.

[19] T.C. Nugent, M. El-Shazly, Chiral amine synthesis - recent developments and trends for enamide reduction, reductive amination, and imine reduction, Adv. Synth. Catal. 352 (2010) 753–819, https://doi.org/10.1002/adsc.200900719.

[20] M. Pera-Titus, F. Shi, Catalytic amination of biomass-based alcohols, ChemSusChem 7 (2014) 720–722, https://doi.org/10.1002/cssc.201301095.

[21] K. Zhou, H. Liu, H. Shu, S. Xiao, D. Guo, Y. Liu, Z. Wei, X. Li, A comprehensive study on the reductive amination of 5-hydroxymethylfurfural into 2,5-bisaminomethylfuran over raney Ni through DFT calculations, ChemCatChem 11 (2019) 2649–2656, https://doi.org/10.1002/cctc.201900304.

[22] M. Chatterjee, T. Ishizaka, H. Kawanami, Reductive amination of furfural to furfurylamine using aqueous ammonia solution and molecular hydrogen: an environmentally friendly approach, Green Chem. 18 (2016) 487–496, https://doi.org/10.1039/C5GC01352F.

[23] G. Liang, A. Wang, L. Li, G. Xu, N. Yan, T. Zhang, Production of primary amines by reductive amination of biomass-derived aldehydes/ketones, angew, Chemie Int. Ed. 56 (2017) 3050–3054, https://doi.org/10.1002/anie.201610964.

[24] T. Komanoya, T. Kinemura, Y. Kita, K. Kamata, M. Hara, Electronic effect of ruthenium nanoparticles on efficient reductive amination of carbonyl compounds, J. Am. Chem. Soc. 139 (2017) 11493–11499, https://doi.org/10.1021/jacs.7b04481.

[25] D. Deng, Y. Kita, K. Kamata, M. Hara, Low-temperature reductive amination of carbonyl compounds over Ru deposited on Nb 2 O 5 • n H 2 O, ACS Sustain. Chem. Eng. 7 (2019) 4692–4698, https://doi.org/10.1021/acssuschemeng.8b04324.

[26] D. Chandra, Y. Inoue, M. Sasase, M. Kitano, A. Bhaumik, K. Kamata, H. Hosono, M. Hara, A high performance catalyst of shape-specific ruthenium nanoparticles for production of primary amines by reductive amination of carbonyl compounds, Chem. Sci. 9 (2018) 5949–5956, https://doi.org/10.1039/C8SC01197D.

[27] H. Yuan, J.-.P. Li, F. Su, Z. Yan, B.T. Kusema, S. Streiff, Y. Huang, M. Pera-Titus, F. Shi, Reductive amination of furanic aldehydes in aqueous solution over versatile Ni y AlO x catalysts, ACS Omega 4 (2019) 2510–2516, https://doi.org/10.1021/acsomega.8b03516.

[28] Y. Zhang, H. Yang, Q. Chi, Z. Zhang, Nitrogen-doped carbon-supported nickel nanoparticles: a robust catalyst to bridge the hydrogenation of nitriles and the reductive amination of carbonyl compounds for the synthesis of primary amines, ChemSusChem 12 (2019) 1246–1255, https://doi.org/10.1002/cssc.201802459.

[29] Z. Yuan, B. Liu, P. Zhou, Z. Zhang, Q. Chi, Preparation of nitrogen-doped carbon supported cobalt catalysts and its application in the reductive amination, J. Catal. 370 (2019) 347–356, https://doi.org/10.1016/j.jcat.2019.01.004.

[30] X. Jv, S. Sun, Q. Zhang, M. Du, L. Wang, B. Wang, Efficient and mild reductive amination of carbonyl compounds catalyzed by dual-function palladium nanoparticles, ACS Sustain. Chem. Eng. 8 (2020) 1618–1626, https://doi.org/10.1021/acssuschemeng.9b06464.

[31] C. Xie, J. Song, M. Hua, Y. Hu, X. Huang, H. Wu, G. Yang, B. Han, Ambient-temperature synthesis of primary amines via reductive amination of carbonyl compounds, ACS Catal. 10 (2020) 7763–7772, https://doi.org/10.1021/acscatal.0c01872.

[32] A.B. Boricha, H.M. Mody, H.C. Bajaj, R.V. Jasra, Hydrogenation of benzene over ruthenium-exchanged montmorillonite in the presence of thiophene, Appl. Clay Sci. 31 (2006) 120–125, https://doi.org/10.1016/j.clay.2005.09.003.

[33] S. Peng, X. Fan, J. Zhang, F. Wang, A highly efficient heterogeneous catalyst of Ru/MMT: preparation, characterization, and evaluation of catalytic effect, Appl. Catal. B Environ. (2013) 115–124, https://doi.org/10.1016/j.apcatb.2013.03.029, 140-141.

[34] A.M. Hengne, B.S. Kadu, N.S. Biradar, R.C. Chikate, C.V. Rode, Transfer hydrogenation of biomass-derived levulinic acid to γ-valerolactone over supported Ni catalysts, RSC Adv. 6 (2016) 59753–59761, https://doi.org/10.1039/C6RA08637C.

[35] K.M. Eblagon, S.C.E. Tsang, Structure-reactivity relationship in catalytic hydrogenation of heterocyclic compounds over ruthenium black-Part A: effect of substitution of pyrrole ring and side chain in N-heterocycles, Appl. Catal. B Environ. (2014) 22–34, https://doi.org/10.1016/j.apcatb.2014.04.044, 160-161.

[36] N. Hussain, P. Gogoi, P. Khare, M.R. Das, Nickel nanoparticles supported on reduced graphene oxide sheets: a phosphine free, magnetically recoverable and cost effective catalyst for Sonogashira cross-coupling reactions, RSC Adv. 5 (2015) 103105–103115, https://doi.org/10.1039/C5RA22601E.

[37] C. Bernardon, M. Ben Osman, G. Laugel, B. Louis, P. Pale, Acidity versus metal-induced Lewis acidity in zeolites for Friedel-Crafts acylation, Comptes Rendus Chim. 20 (2017) 20–29, https://doi.org/10.1016/j.crci.2016.03.008.

[38] K.D. Kim, Z. Wang, Y. Jiang, M. Hunger, J. Huang, The cooperative effect of Lewis and Brønsted acid sites on Sn-MCM-41 catalysts for the conversion of 1,3-dihydroxyacetone to ethyl lactate, Green Chem. 21 (2019) 3383–3393, https://doi.org/10.1039/C9GC00820A.

[39] G.B. Kasar, R.S. Medhekar, P.N. Bhosale, C.V. Rode, Kinetics of hydrogenation of aqueous levulinic acid over bimetallic Ru-Ni/MMT catalyst, Ind. Eng. Chem. Res. 58 (2019) 19803–19817, https://doi.org/10.1021/acs.iecr.9b03748.

[40] S. Pichaikaran, P. Arumugam, Vapour phase hydrodeoxygenation of anisole over ruthenium and nickel supported mesoporous aluminosilicate, Green Chem. 18 (2016) 2888–2899, https://doi.org/10.1039/C5GC01854D.

[41] V.V. Kumar, G. Naresh, M. Sudhakar, J. Tardio, S.K. Bhargava, A. Venugopal, Role of Brønsted and Lewis acid sites on Ni/TiO_2 catalyst for vapour phase hydrogenation of levulinic acid: kinetic and mechanistic study, Appl. Catal. A Gen. 505 (2015) 217–223, https://doi.org/10.1016/j.apcata.2015.07.031.

[42] P. KOOPMAN, Characterization of ruthenium catalysts as studied by temperature programmed reduction, J. Catal. 69 (1981) 172–179, https://doi.org/10.1016/0021-9517(81)90139-1.

[43] S. Galvagno, G. Capannelli, G. Neri, A. Donato, R. Pietropaolo, Hydrogenation of cinnamaldehyde over Ru/C catalysts: effect of Ru particle size, J. Mol. Catal. 64 (1991) 237–246, https://doi.org/10.1016/0304-5102(91)85115-I.

[44] C. Rong, X. Ding, Y. Zhu, Y. Li, L. Wang, Y. Qu, X. Ma, Z. Wang, Production of furfural from xylose at atmospheric pressure by dilute sulfuric acid and inorganic salts, Carbohydr. Res. 350 (2012) 77–80, https://doi.org/10.1016/j.carres.2011.11.023.

[45] R. Suxia, X. Haiyan, Z. Jinling, L. Shunqing, H. Xiaofeng, L. Tingzhou, Furfural production from rice husk using sulfuric acid and a solid acid catalyst through a two-stage process, Carbohydr. Res. 359 (2012) 1–6, https://doi.org/10.1016/j.carres.2012.07.006.